Published in final edited form as:
Circ Cardiovasc Imaging. 2013 March 1; 6(2): 285–294. doi:10.1161/CIRCIMAGING.112.000119.

Dual-Energy Computed Tomography Imaging of Atherosclerotic Plaques in a Mouse Model Using a Liposomal-Iodine Nanoparticle Contrast Agent

Rohan Bhavane, PhD[1], **Cristian Badea, PhD**[2], **Ketan B. Ghaghada, PhD**[1], **Darin Clark, BS**[2], **Deborah Vela, MD**[3], **Anoosha Moturu**, **Akshaya Annapragada**, **G. Allan Johnson, PhD**[2], **James T. Willerson, MD**[3], and **Ananth Annapragada, PhD**[1]

[1]Texas Children's Hospital, The Singleton Department of Pediatric Radiology, Houston, TX

[2]Duke University, Department of Radiology, Durham, NC

[3]The Texas Heart Institute, Houston, TX

Abstract

Background—The accumulation of macrophages in inflamed atherosclerotic plaques has been long recognized. In an attempt to develop an imaging agent for detection of vulnerable plaques, we evaluated the feasibility of a liposomal-iodine nanoparticle contrast agent for computed tomography (CT) imaging of macrophage-rich atherosclerotic plaques in a mouse model.

Methods and Results—Liposomal-iodine formulations varying in particle size and polyethylene glycol coating were fabricated, and shown to stably encapsulate the iodine compound. *In vitro* uptake studies using optical and CT imaging in the RAW264.7 macrophage cell line identified the formulation that promoted maximal uptake. Dual-energy CT imaging using this formulation in Apolipoprotein E deficient ($ApoE^{-/-}$) mice (n=8) and control C57BL/6 mice (n=6) followed by spectral decomposition of the dual-energy images enabled imaging of the liposomes localized in the plaque. Imaging cytometry confirmed the presence of liposomes in the plaque and their co-localization with a small fraction (~2%) of the macrophages in the plaque.

Conclusions—The results demonstrate the feasibility of imaging macrophage-rich atherosclerotic plaques using a liposomal-iodine nanoparticle contrast agent and dual-energy CT.

Keywords

liposome; contrast media; atherosclerosis; computed tomography; macrophage

The progression of atherosclerotic deposits from their early beginnings (the so-called fatty streak) to the formation of mature plaques with a fibrous cap, the accumulation of macrophages behind the fibrous cap, the potential for plaque rupture (the so-called vulnerable plaques) and the formation of stable, calcified plaques, are all reported

Correspondence to: Ananth Annapragada, Professor and Director of Basic Research, The Singleton Department of Pediatric Radiology, 1102 Bates Avenue, Suite 850, Texas Children's Hospital, Houston, TX 77030, Phone: 832-824-0865, Fax: 832-825-0260, avannapr@texaschildrens.org.

Disclosures
AA and KBG are both significant stockholders in Marval Biosciences Inc.

extensively in the literature.[1–5] Of these phases, the vulnerable plaque is the most feared, because of the usually catastrophic consequences of plaque rupture: the thrombus lodging at the site of rupture and associated dynamic vasoconstriction leading to acute obstructions of blood flow, often leading in turn, to an acute myocardial infarction or a stroke.[6] The detection of atherosclerotic plaques, and the identification of vulnerable plaques among them, is therefore a much sought-after goal.

Some of the key features of high-risk plaques include the presence of a large necrotic core with a thin fibrous cap (< 65 μm) consisting mostly of type 1 collagen with few smooth muscle cells.[3–5] In addition, detailed histological studies have demonstrated that a significant cause of plaque vulnerability is the accumulation of macrophages behind the fibrous cap of the plaque, attracted to the site by inflammation surrounding the plaque as it protrudes into the blood stream[7]. Targeting inflammatory response, the macrophages recruited to the site, or the receptors that participate in the recruitment, are viable methods to target vulnerable plaques. Several attempts have been made to develop contrast agents enabling non-invasive imaging of macrophage-rich plaques. These include agents for use with nuclear imaging,[8, 9] optical imaging,[10] magnetic resonance imaging,[11] and X-ray imaging.[12] In addition, signal-amplification strategies using nanoparticle platforms have also been investigated.[13–17] While they are all presumably being readied for the clinic, one expects that their progress would be slowed by the relative dearth of clinical safety data for these particle platforms.

In this work, we evaluated the feasibility of a liposomal iodinated contrast agent for CT imaging of macrophage-rich plaques in a mouse model of atherosclerosis. We hypothesized that a liposomal nanoparticle encapsulating a large payload of iodinated contrast agent would localize sufficient iodine in macrophage-laden plaques to enable *in vivo* imaging. The choice of a liposomal platform for development of a CT contrast agent was based on the following: (1) extensive historical data on clinical use,[18] and (2) capacity to encapsulate a large payload of clinically-used iodine contrast agent molecules.[19, 20]

Methods

Materials

1,2-Dipalmitoyl-sn-Glycero-3-Phosphatidylcholine (DPPC), Cholesterol (Chol), 1,2-Dipalmitoyl-sn-Glycero-3-phosphoglycerol, sodium salt (DPPG), were purchased from Avanti Polar lipids (Alabaster, AL, USA). N-(carbonyl-methoxy polyethylene glycol 2000)-1,2-Distearoyl-sn-Glycero-3 phosphoethanolamine (mPEG-2000-DSPE) was purchased from Genzyme Pharmaceuticals (Cambridge, MA, USA). Lissamine™ rhodamine B 1,2-dihexadecanoyl-*sn*-glycero-3-phosphoethanolamine triethylammonium salt (rhodamine-DHPE) was purchased from Invitrogen Corp. (Carlsbad. CA, USA). MTS-based cell viability assay kit was purchased from Promega Corp. (Madison, WI, USA). RAW 264.7 murine macrophages were obtained from ATCC (Manassas, VA, USA). Whatman Nuclepore polycarbonate track-etch membranes of 100, 200, and 400 nm pore sizes were purchased from Fisher Scientific (Waltham, MA, USA). Common laboratory reagents and cell culture medium were obtained from Sigma-Aldrich (St. Louis, MO, USA), VWR International (West Chester, PA, USA), and Fisher Scientific.

Preparation of Liposomal Formulations

Two types of liposomal formulations were prepared: (1) rhodamine-labeled liposomes used in fluorescent-based cell culture experiments and (2) liposomal-iodixanol used for *in vitro* CT imaging of cells and *in vivo* studies in mice. Liposomes were prepared using extrusion methods as described previously.[19] To study the effect of surface coating on macrophage

uptake, two surface compositions of liposomes were chosen: PEGylated liposomes, liposomes containing 3% polyethylene glycol (PEG), and non-PEGylated liposomes (Table 1). DPPG, a charged lipid, was included in the non-PEG liposomes to prevent liposome aggregation in the absence of PEG.

To prepare the formulations, lipids were dissolved in ethanol (10% of total volume) and then hydrated with 10 mM Tris saline buffer (pH 7.2) or iodixanol solution (400 mg I/ml) for 30 minutes with constant stirring at 60–65 °C. The hydrated lipids were then extruded 7 – 10 times at 65 °C through either a 400, 200 or 100 nm Nuclepore membrane using a high-pressure extruder (Northern Lipids, Vancouver, BC, Canada) thus forming liposomes over a range of sizes.

The liposomal suspensions were diafiltered using a MicroKros module (Spectrum Laboratories Inc., CA, USA, 500 kDa molecular weight cutoff) to remove un-encapsulated iodixanol. The iodine concentration was determined by UV spectrometry (λ = 245 nm) using a blank liposome suspension to correct for background absorbance due to scattering. Total phospholipid content of the liposomal formulations was determined by measuring total phosphorus using inductively-coupled plasma atomic emission spectroscopy (ICP-AES).

The size and charge of the liposomes was determined using a Brookhaven Instruments Dynamic Light Scattering instrument (Brookhaven Instruments Corp., Holtsville, NY, USA). The zeta potential of the liposomes was measured in 10 mM Tris at pH ~ 7.2. The size measurement was performed in tris-buffered saline at pH ~ 7.2.

The *in vitro* stability of liposomal-iodine was tested in bovine plasma. Briefly, liposomes were incubated with plasma at 37 °C for 90 minutes. The mixture was then dialyzed against 150 mM saline using a 10,000 MWCO membrane at room temperature. The external phase was analyzed periodically by UV-Vis spectrometry (λ_{Abs}=245 nm) for the next 20 hours to determine the amount of iodine that leaked out of the liposomes. As a control, plasma of equal volume was dialyzed to rule out absorbance from plasma components that could appear in the external phase.

Cell Culture and Microscopy

Uptake of Fluorescent Liposomes by RAW 264.7 Macrophages—RAW 264.7 macrophages were plated on 8 chamber glass slides (~20,000 cells per well) supplemented with DMEM containing 10 % fetal bovine serum (FBS) and 1% antibiotics. After 24 hours, the medium was replenished with fresh medium, and the adherent cells were incubated with the rhodamine-labeled liposomal formulations for 2, 4, 6, 10, 18, 24 and 36 hours at 750 μM lipid concentration.

At the end of the incubation period, the medium was discarded followed by gentle washes twice with DMEM and 3 times with phosphate buffered saline (PBS). The cells were fixed with cold 4% para-formaldehyde in PBS for 5 minutes. They were washed 3 times with PBS and incubated with 0.1% Triton X-100 PBS containing 1% BSA for 5 minutes. The cells were finally washed with PBS and incubated with mounting medium containing 4',6-diamidino-2-phenylindole (DAPI) for nuclear staining. The slides were cover-slipped and imaged by epifluorescent microscopy.

Image-based cytometry of liposome uptake in vitro was performed using the Lipid Droplet Algorithm on CyteSeer (Vala Sciences, San Diego CA). The average pixel intensity in the rhodamine channel associated with each cell was determined. The mean and standard deviation were calculated over all imaged cells in each preparation. The Student's double-tailed t-test with the Bonferroni correction for multiple testing was then used to determine if

the uptake levels for the 3 preparations (100nm, 200nm, 400nm) in each group (PEG, non-PEG) at each time point were significantly different (H0: μ1=μ2) from each other. Differences at the 95% confidence level (uncorrected $p<0.05$) were considered significant.

CT detection of Liposomal-iodine Uptake by RAW 264.7 Macrophages—RAW 264.7 macrophages were plated in standard 6 well plates (~ 200,000 cells/well) supplemented with DMEM complete medium containing 10 % FBS and 1% antibiotics. After 24 hours, the medium was replenished with fresh medium, and the adherent cells were incubated with liposomal-iodixanol formulations for 2, 4, 10, and 24 hours at 750 μM lipid concentration.

At the end of each incubation time point, the medium was discarded and the adherent cells rinsed twice with fresh DMEM. The cells were then detached using a cell scraper and centrifuged at 150 g for 5 minutes. The cell pellet was re-suspended in DMEM and cells were counted on a hemocytometer. A cell suspension volume corresponding to approximately 2 million cells was collected in a micro-centrifuge and centrifugally separated. The resulting cell pellet was then stored in PBS at 4 °C for upto 24 hours prior to CT imaging.

Imaging was performed on a GE pre-clinical CT scanner. The following parameters were used for the scans: beam energy of 80 kVp, tube current of 450 μA, an exposure time of 500 milliseconds, a spatial resolution of 92 μm, and 360 projections. The scan time was 10 minutes.

Quantitative analysis of *in vitro* CT images was performed in OsiriX (v. 3.6, 64 bit). Three regions of interest (ROI) were drawn in each cell pellet. The image intensity was recorded in Hounsfield Units. The Student's double-tailed t-test with the Bonferroni correction for multiple testing was used to test if the measured uptake of particles was significantly different (H0: μ1=μ2) between each of the 3 preparations (100, 200, 400nm) in each group (PEG, non-PEG) at each time point. Differences at the 95% confidence level (uncorrected $p<0.05$) were considered significant.

Cell Viability after Incubation with Liposomal-iodine—To determine the viability of cells after incubation with liposomes, a MTS assay (CellTiter 96® Aqueous Non-Radioactive Cell Proliferation Assay, Promega, Madison, WI, USA) was performed following instructions on the kit. Briefly, the assay uses a solution of [3-(4,5-dimethylthiazol-2-yl)-5-(3-carboxymethoxyphenyl)-2-(4-sulfophenyl)-2H-tetrazolium, inner salt; MTS] that is bio-reduced by live cells to form a formazan product that is soluble in cell culture medium.

About 4000 cells per well were plated in a 96 well black–walled plate with clear bottom. Half of the medium (DMEM) was replaced the next day with fresh medium. The cells were then incubated initially in DMEM, and then spiked with a liposomal-iodixanol formulation (750 μM of lipids in each well) for 2, 6, 24, and 36 hours. The total incubation period for each well (time in DMEM + time with formulation) was held constant at 36 hours. Untreated controls were prepared identically, except no liposomes were present in the sham spike. At the end of the incubation period, the medium was discarded, and the adherent cells were gently rinsed with fresh medium. The cells were then incubated with freshly prepared MTS solution. The absorbance of the formazan product at 490 nm was measured, and is directly proportional to the number of living cells. The cell viability was determined by the following formula, %Viability = (absorbance of cells treated with liposomes/ average absorbance of untreated cells) × 100. Results were presented as mean values of treatments (n=3) with the error bars indicating standard deviations. The Student's double-tailed t-test

was used to test the significance of difference of each treatment group (H0: $\mu 1=\mu 2$) individually from the untreated control group (n=6). Any value of $p<0.05$ was considered significant.

Animal Studies

All animal procedures were approved by the Institutional Animal Care and Use Committees at Duke University Medical Center, and University of Texas Health Science Center, Houston. Eight ApoE$^{(-/-)}$ mice (12 ± 2 months) and six control C57BL/6 mice were used for the study. The ApoE$^{(-/-)}$ animals were fed with a Western type diet for 4–12 weeks prior to CT imaging studies.

The imaging studies were performed on a custom-built dual source micro-CT system described previously[21] using 40 kVp, 250mA, 16 ms per exposure for one imaging chain and 80 kVp, 160mA, 10 ms for the other imaging chain. For each imaging set 360 projections were acquired over a complete rotation. The two x-ray tubes fired simultaneously. Mice were kept anesthetized with 1.5% isoflurane during scanning. Temperature was maintained with heat lamps and a feedback controller. A prospective two-channel gating method was used to eliminate both respiratory and cardiac motion during scanning.[22] The ECG signal was monitored from the footpads while the pulmonary signal was monitored with a pneumatic pillow. Both signals were integrated for gating using a custom LabVIEW script. CT images were acquired at 4 time points: pre-contrast injection, and 2, 48, and 96 hours post-contrast injection. Liposomal-iodixanol contrast agent was injected into the tail vein at 20μL/gm (1.4 mg of I/gm body weight) over 2 – 3 minutes. We did not include a control group with free iodixanol injection (instead of the liposomal iodixanol) because there is no evidence of ulceration or rupture of plaques in ApoE−/− mice in the age range of our study, and free iodixanol does not localize in plaques in the absence of ulceration.[23]

CT reconstructions were performed using the Feldkamp algorithm resulting in two CT data sets (512×512x512 matrix size and 88 microns voxel size) corresponding to the two source energies at each imaging time point.[24] Each of the two CT sets was first processed using edge-preserving bilateral filtering to reduce noise and then used to perform a dual energy material-decomposition using scripts written in MATLAB as described previously.[25, 26] Based on the decomposition, 3D iodine and calcium concentration maps were generated. Color-coded decomposed images displaying either iodine or calcium signal or fused iodine-calcium signal were generated using ImageJ (NIH, v1.46a 64-bit).

Ex vivo studies of liposome uptake in plaques

The liposomes injected into ApoE$^{(-/-)}$ and C57BL/6 mice for CT imaging also contained rhodamine. After CT imaging, the mice were sacrificed, and perfused with phosphate buffered saline. The aortas were excised and fixed in 4% para-fomaldehyde for 3–4 hours and then incubated in 30% sucrose solution for 24 hours. The aortas were then cut and embedded in OCT and frozen at −80 °C. 10 μm thick sections were cut from the frozen blocks on a cryotome and mounted on glass slides. The slides were then stained with a nuclear stain (DAPI) and FITC-labeled Mac-2 antibody, for macrophages, and imaged in the DAPI, rhodamine and FITC channels on an epifluorescent microscope. The incident light intensity and camera exposure settings for each channel were kept constant for all the sections imaged.

Aorta sections from ApoE$^{(-/-)}$ animals fed normal chow and not treated with rhodamine liposomes were also imaged in the same 3 channels as a control group to account for any background fluorescence (in the rhodamine channel) associated with the plaques.

The images were processed using ImageJ (v1.46r 64 bit) and Fiji (v1.47b 64 bit) to crop out any areas not associated with intimal tissue or plaques. The excluded areas were either sections of the vessel wall (media, adventitia) or vessel lumen. The cropped images were then analyzed in CyteSeer (Vala Sciences, San Diego CA) using the Colocalization algorithm. Cyteseer operates by identifying individual nuclei (via the signal in the DAPI channel) and tessellating the remaining space into individual cells, each cell containing one nucleus. Artifactual cells in the whitespace surrounding the cropped images were then manually removed from the analysis. The average FITC channel intensity of each cell was then plotted against the average rhodamine intensity for image-based cytometry.

Results

Characterization of Liposomal Formulations

The non-PEG liposomes, containing the negatively charged lipid - DPPG, showed 1.5 – 2 fold higher surface negative charge compared to their PEG counterparts (Table 2). The rhodamine-labeled liposomes exhibited particle sizes similar to those seen previously for liposomes of similar compositions extruded through the filter pore sizes used in this study.[27] The use of highly concentrated and viscous iodixanol solution impacted particle size when compared with rhodamine-labeled liposomes that were extruded in a non-iodinated buffer solution. The liposomal formulations extruded through the 400nm filter membranes, due to their high encapsulation volume, showed the largest iodine to lipid ratio (Table 3). *In vitro* stability analysis of liposomal iodixanol formulations in bovine plasma demonstrated stable encapsulation of iodixanol as shown by less than 2 % free iodixanol measured over 20 hours of dialysis. (Supplemental Figure 1)

Fluorescent Uptake Studies with RAW 264.7 Macrophages

To study macrophage uptake of PEGylated and non-PEGylated liposomes, rhodamine-labeled liposomes were incubated with RAW 264.7 murine macrophages. The non-PEGylated liposomal formulations were taken up more avidly than PEGylated liposomal formulations (Figure 1). Quantitative analysis of fluorescent images demonstrated that the non-PEG liposomal formulation extruded through 400 nm filter membrane, showed a significantly higher uptake after 6 hours when compared to 100 and 200 nm non-PEG liposomes (Figure 2A). An increase in signal intensity was seen with incubation time for all the liposomal formulations. While the PEG-liposomes exhibited a positive correlation between macrophage uptake and incubation period, no significant differences in uptake were seen among various sizes (Figure 2B).

CT uptake studies with RAW 264.7 Macrophages

In order to evaluate the feasibility of detecting macrophages containing nanoparticle contrast agent using CT imaging, non-PEGylated and PEGylated liposomes containing the iodine contrast agent iodixanol were incubated with RAW 264.7 macrophages for different incubation periods. No detectable signal was seen at the 2-hour incubation period for any of formulations. At 4 hours, only the cells incubated with non-PEGylated 400 nm liposomes showed detectable signal. After 24 hours of incubation, all the pellets showed detectable signal. At the 24-hour point, the 400 nm non-PEG liposomes showed significantly higher uptake with a CT number of 600 HU (Figure 2C). In comparison, the CT number in a blank pellet was 6 ± 2.2 HU. Based on the in vitro results, the non-PEG liposomal formulation extruded through 400 nm membrane was used for in vivo testing.

MTS Assay for Cell Viability

The viability of the cells after incubation with liposomal-iodixanol was determined by MTS assay. While sporadic samples showed statistically different cell viability compared to the control as indicated by the p-values, no particular trend was observed either with increased incubation time or differences in formulation suggesting that the liposomal formulations had little to no effect on the viability of cells (Figure 3).

***In vivo* Studies—**Animals were imaged on a dual source micro-CT scanner before and after injection of rhodamine containing liposomal-iodixanol contrast agent. All the 8 ApoE$^{(-/-)}$ animals scanned in this study, showed some level of calcification in the aorta. Animals were imaged at 40 and 80 kVp to enable spectral decomposition of images for separation of iodine and calcium signal. The high blood-pool signal attenuation obtained immediately post-contrast facilitated clear visualization of the vessel lumen in areas adjacent to calcified plaques (Figure 4). By 48 hours, the majority of contrast agent was cleared from systemic circulation as demonstrated by the absence of any residual blood-pool enhancement. The use of spectral imaging enabled detection of iodine signal in areas of calcified plaques (Figure 5). The iodine signal was visible at several regions in the aorta, most notably the aortic arch and aortic sinus. CT imaging of control mice did not demonstrate non-specific signal enhancement in any regions of the aorta (Figure 5). Additional images from the other animals are provided in supplementary data.

Ex vivo studies of liposome uptake in plaques—To analyze the extent of macrophage uptake of the rhodamine liposomes, aortic sections were stained for macrophage and cell nucleus and imaged using fluorescent microscopy. Localization of rhodamine label appeared consistently but was weak in all areas of concentrated macrophage populations at exposed regions of plaques as well as in smooth muscle of the vascular wall proximal to the lumen. Figure 6 shows a representative section of plaque infiltrated with macrophages and with rhodamine liposomes localized in the plaque.

Image based cytometric analysis by tesselating the image into approximations of cell boundaries as in Figure 6D is shown in Figure 7. Each point represents the mean rhodamine and FITC intensity within each such approximate cell. Tissues from normal mice showed low levels of macrophages and low rhodamine signal (blue points). ApoE$^{-/-}$ mice not treated with Rhodamine labeled liposomes (black points) showed a greater level of macrophages, as expected since they have significant plaque buildup. However, their rhodamine signal was only marginally higher, and is attributed to tissue background. ApoE −/− mice treated with Rhodamine liposomes however, showed a distinct population of macrophage cells in which high levels of rhodamine label are observed (red points). This population is clearly distinct from the C57BL/6 control (normal) mice and the ApoE$^{(-/-)}$ control mice not treated with rhodamine labeled liposomes. The fraction of cells showing the elevated rhodamine levels is relatively small, ~2%.

Discussion

Macrophages play a central role in the development and progression of atherosclerotic plaques. As they engulf lipid deposits behind the fibrous cap, macrophages transform into foam cells, and apparently, many of them remain in situ, contributing in part to a swelling of the plaque, further inflammation, and a cascade to even more rapid macrophage recruitment to the site. Atheroma macrophage burden is known to increase continuously from plaque erosion to plaque rupture.[28] Quantitative analysis of macrophage burden and atherosclerotic plaque progression has primarily been investigated using histological techniques. A semi-quantitative, immunohistological analysis of macrophages in plaques, as a function of age,

showed that macrophages occupied 40–60% of plaque area.[29] Systemic infections have also been shown to enhance inflammation at sites of plaque, causing an increase in macrophage infiltration both within the plaque and the surrounding adventitia. In several cases, the infections result in acute myocardial infarction and deaths. Madjid et al[30] used histological analysis to show that patients with influenza infection had twice as many macrophages (582 ± 774 per mm^2) in atheromatous lesions than control subjects (281 ± 321 per mm^2) with atherosclerosis and no infection. The number of macrophages in the adventitial layer was 5 times more in infected cases (1577 ± 1872 per mm^2) than the control cases (265 ± 185 per mm^2). Non-invasive imaging techniques that enable quantitative analysis of plaque macrophage burden could therefore assist in identification of these so-called 'vulnerable' patients.

Positron-emission tomography (PET) imaging using ^{18}F-FDG has been investigated, both pre-clinically and clinically, to assess macrophage burden. However, the low-spatial resolution and limited specificity present challenges inspite of its high contrast sensitivity.[31] CT and MRI provide relatively high spatial resolution compared to PET imaging. MRI also has the advantage of far higher sensitivity when compared to CT. However, quantitative analysis of MR images is challenging because of the lack of linearity in signal intensity and contrast agent concentration. CT is better suited for quantitative imaging since signal attenuation is directly proportional to contrast agent concentration. However, most CT systems clinically installed today provide very limited material discrimination due to the use of a single energy in scanning. Due to this limitation, calcified deposits, which are frequently observed in atherosclerotic plaques and result in high signal attenuation, may be indistinguishable from iodinated contrast agents that accumulate at these sites. The low contrast sensitivity of CT technique is further accentuated by the limitations of conventional iodine-based contrast agents, namely, lack of target specificity and signal amplification capabilities since a single targeting molecule can only be associated with a single imaging moiety, in this case iodine. Recent advances in spectral CT imaging using dual-energy CT scanners and fast scanning voltages (kVp) switching have the potential to overcome these issues.[32]

In this pre-clinical study, we therefore used CT as the mode of detection and a liposomal-iodinated contrast agent for providing target specificity and signal amplification for imaging of macrophage-rich plaques. Liposomes have been used as drug delivery vehicles for nearly 20 years, with the major use being in the delivery of chemotherapeutics to solid tumors.[33] Recently, both CT and MR imaging agents using PEGylated liposomes as carriers for the imaging agents have been demonstrated.[19, 20, 34, 35] The primary clearance route of these particles from the bloodstream is via the reticulo-endothelial system (RES), and as such, their presence in circulatory macrophages that localize into atherosclerotic plaques is quite likely. However, their long circulation half-life (~40 hours) implies that the localized particles are not likely to be visible in a CT scan over the background of the residual particles in the bloodstream.[36] In order to develop a short blood-half life contrast agent, a non-PEGylated liposomal construct was considered. A reduction in the PEG levels would also accelerate the macrophage uptake rate of these particles. In addition, previous studies have shown that the macrophage uptake rate is dependent on the size of liposome particles.[37] We therefore chose to vary the particle size and select a particle size that maximizes the macrophage uptake rate. The choice of iodine as the imaging moiety was based on the availability of clinical data with iodinated contrast agents (in this work, iodixanol was encapsulated in the liposomes). Other studies have demonstrated the use of higher Z elements, specifically gold and bismuth, for development of X-ray contrast agents.[16, 38, 39] While such agents have greater attenuation efficiency, the lack of safety and toxicity data, both in pre-clinical and clinical testing, presents challenges for clinical translation.

In vivo imaging studies were performed on a dual-energy micro-CT scanner to enable material discrimination. In the ApoE deficient model, calcified plaques typically develop after about 6 – 8 months of age.[40] A two-energy spectral separation technique was therefore developed to differentiate calcium deposits from iodine based on the differences in their X-ray absorption spectra.[25]. Briefly, a post-reconstruction dual energy decomposition was applied to the CT data, resulting in independent images of iodine and calcium. The selection of the two scanning energies was based on simulations and validated in phantom studies, to maximize the selectivity between the two images. For the dual source micro-CT system, 40 kVp is the lowest voltage allowed by the CT system's X-ray generator. This voltage provides minimum enhancement while values in the range of 70 or 80 kVp provide maximum enhancement when imaging Iodine. Calcium, on the other hand, has a maximum CT attenuation at 40 kVp and this monotonically decreases with an increase in kVp. Therefore, in the ApoE$^{(-/-)}$ mice studies, we selected 40 and 80 kVp as the scanning energies to optimize contrast discrimination between calcium and iodine. With a dual energy scan and elemental decomposition, it was possible to separate the signal between calcium and any iodine that may be taken up macrophages. The presence of iodine in the plaque can be attributed both to uptake of the liposomes by macrophages residing in the plaque and to circulating macrophages that have taken up liposomes and trafficked into the plaque lesions. Swirski et al[41] have shown that certain populations of splenic monocytes can be recruited into inflamed regions of the aorta, suggesting that macrophages from the RES could also contribute. In the ApoE−/− model, our data suggests that it takes at least 48 hours for a detectable number of liposomes (or macrophages loaded with liposomes) to enter inflamed plaque.

Image based cytometric analysis of the atherosclerotic lesions suggests that the lesions are rich in macrophages, consistent with their inflamed status, and that the iodine-containing liposomes are localized in a small fraction of these macrophages. This small fraction is consistent with the relatively short duration of time for which the animals were exposed to the particles, and that the macrophages had to take up the particles and be transported to the lesion. However, this relatively small number of macrophages still contain enough iodinated liposomes to be readily detected by CT imaging.

The limitations of this work include the small feature size in mice and the need to use a micro-CT system, making clinical translation difficult due to differences both in pathophysiology and imaging hardware.[42, 43] Lacking an HU calibration on this scanner, we were unable to quantify the plaques observed. Before starting clinical trials, testing in larger animal species on clinical CT scanners will be necessary. Second, the surface charge on DPPG liposomes has the potential for eliciting hypersensitivity reactions.[44] Studies to evaluate the potential toxicity of these agents are clearly warranted and will be required for an investigational new drug application. Third, in addition to their enhanced uptake by macrophages, the non-PEGylated 400 nm liposomes also carry a greater amount of iodine per unit of lipid in comparison to typical liposomal formulations. However, the size of particles may pose challenges in sterilization, and aseptic processing may be necessary to manufacture a sterile product for clinical use. Fourth, the current generation of clinical CT scanners do not enable imaging below 80 kVp, although spectral decomposition techniques to separate calcium from iodine at standard clinical energies have been investigated.[32] Furthermore, challenges still remain due to small feature sizes, large voxel size on clinical CT systems and the potential for partial volume effects, resulting in limited contrast sensitivity. However, the technological advances in dual-energy CT scanners, with respect to material discrimination, photon counting detectors, low radiation dose and increased spatial resolution, coupled with improved image processing techniques for noise reduction are likely to have a positive impact on the use of CT for quantifying and detecting vulnerable plaques.[16] There is also growing evidence in the literature for the role of

macrophages in other diseases with inflammatory processes,[5, 45, 46] all of which could be imaged using the methods presented in this paper. In summary, in the short term, the methods described in this study are appealing for investigational use, but their use in humans will have to wait for regulatory approval.

Supplementary Material

Refer to Web version on PubMed Central for supplementary material.

Acknowledgments

The authors would like to acknowledge Dr. Yi Qi (Duke University) and Dr. Laurence Hedlund for help with the animal studies; Tommy Reese and Betsy Molinari (Texas Heart Institute) for assistance with histology; Evan Johnson and Charles Kingsley (MD Anderson Cancer Center) for CT imaging of in vitro phantoms; the veterinary staff at UTHSCH and Duke Medical Center. Dr. Zbigniew Starosolski assisted with the 3D volume renderings.

Source of Funding

This work was supported in part by funding from Marval Biosciences Inc. (AA, KBG). Part of this work was supported by NIH/NCRR National Biomedical Technology Resource Center grants (P41 RR005959, NCI U24 CA092656) (CB, GAJ).

References

1. Hansson G. Inflammation, Atherosclerosis, and Coronary Artery Disease. New England Journal of Medicine. 2005; 352:1685–1695. [PubMed: 15843671]
2. Duff G. The pathogenesis of atherosclerosis. Canadian Medical Association Journal. 1951; 64:387–394. [PubMed: 14831039]
3. Virmani R, Burke A, Farb A, Kolodgie F. Pathology of the Unstable Plaque. Progress in Cardiovascular Diseases. 2002; 44:349–356. [PubMed: 12024333]
4. Virmani, R.; Narula, J.; Leon, M.; Willerson, J. The Vulnerable Atherosclerotic Plaque: Strategies for Diagnosis and Management. John Wiley & Sons, Ltd; 2007.
5. Libby P. Inflammation in atherosclerosis. Nature. 2002; 420:868–874. [PubMed: 12490960]
6. Naghavi M, Libby P, Falk E, Casscells SW, Litovsky S, Rumberger J, Badimon JJ, Stefanadis C, Moreno P, Pasterkamp G, Fayad Z, Stone PH, Waxman S, Raggi P, Madjid M, Zarrabi A, Burke A, Yuan C, Fitzgerald PJ, Siscovick DS, Korte CLd, Aikawa M, Airaksinen KEJ, Assmann G, Becker CR, Chesebro JH, Farb A, Galis ZS, Jackson C, Jang IK, Koenig W, Lodder RA, March K, Demirovic J, Navab M, Priori SG, Rekhter MD, Bahr R, Grundy SM, Mehran R, Colombo A, Boerwinkle E, Ballantyne C, Insull W Jr, Schwartz RS, Vogel R, Serruys PW, Hansson GK, Faxon DP, Kaul S, Drexler H, Greenland P, Muller JE, Virmani R, Ridker PM, Zipes DP, Shah PK, Willerson JT. From vulnerable plaque to vulnerable patient: a call for new definitions and risk assessment strategies: part I. Circulation. 2003; 108:1664–1672. [PubMed: 14530185]
7. Virmani R, Burke AP, Farb A, Kolodgie F. Pathology of the Vulnerable Plaque. Journal of the American College of Cardiology. 2006; 47:C13–C18. [PubMed: 16631505]
8. Johnson LL, Schofield L, Donahay T, Narula N, Narula J. 99mTc-Annexin V Imaging for In Vivo Detection of Atherosclerotic Lesions in Porcine Coronary Arteries. The Journal of Nuclear Medicine. 2005; 46:1186–1193.
9. Nahrendorf M, Keliher E, Panizzi P, Zhang H, Hembrador S, Figueiredo J, Aikawa E, Kelly K, Libby P, Weissleder R. 18F-4V for PET-CT Imaging of VCAM-1 Expression in Atherosclerosis. JACC Cardiovascular Imaging. 2009; 2:1213–1222. [PubMed: 19833312]
10. Chen J, Tung C-H, Mahmood U, Ntziachristos V, Gyurko R, Fishman MC, Huang P, Weissleder R. In Vivo Imaging of Proteolytic Activity in Atherosclerosis. Circulation. 2002; 105:2766–2771. [PubMed: 12057992]
11. Botnar RM, Perez AS, Witte S, Wiethoff AJ, Laredo J, Hamilton J, Quist W, Parsons EC, Vaidya A, Kolodziej A, Barrett JA, Graham PB, Weisskoff RM, Manning WJ, Johnstone M. In Vivo

Molecular Imaging of Acute and Subacute Thrombosis Using a Fibrin-Binding Magnetic Resonance Imaging Contrast Agent. Circulation. 2004; 109:2023–2029. [PubMed: 15066940]

12. Hyafil F, Cornily J, Feig J, Gordon R, Vucic E, Amirbekian V, Fisher E, Fuster V, Feldman L, Fayad Z. Noninvasive detection of macrophages using a nanoparticulate contrast agent for computed tomography. Nature Medicine. 2007; 13:636–641.
13. Nahrendorf M, Zhang H, Hembrador S, Panizzi P, Sosnovik D, Aikawa E, Libby P, Swirski F, Weissleder R. Nanoparticle PET-CT Imaging of Macrophages in Inflammatory Atherosclerosis. Circulation. 2008; 117:379–387. [PubMed: 18158358]
14. Ruehm S, Corot C, Vogt P, Kolb S, Debatin J. Magnetic resonance imaging of atherosclerotic plaque with ultrasmall superparamagnetic particles of iron oxide in hyperlipidemic rabbits. Circulation. 2001; 103:415–422. [PubMed: 11157694]
15. Litovsky S, Madjid M, Zarrabi A, Casscells S, Willerson J, Naghavi M. Superparamagnetic iron oxide-based method for quantifying recruitment of monocytes to mouse atherosclerotic lesions in vivo: Enhancement by tissue necrosis factor-α, interleukin-1β, and interferon-γ. Circulation. 2003; 107:1545–1549. [PubMed: 12654614]
16. Cormode DP, Roessl E, Thran A, Skajaa T, Gordon RE, Schlomka JP, Fuster V, Fisher EA, Mulder WJ, Proksa R, Fayad ZA. Atherosclerotic plaque composition: analysis with multicolor CT and targeted gold nanoparticles. Radiology. 2010; 256:774–782. [PubMed: 20668118]
17. Hyafil F, Cornily J, Rudd J, Machac J, Feldman L, Fayad Z. Quantification of Inflammation Within Rabbit Atherosclerotic Plaques Using the Macrophage-Specific CT Contrast Agent N1177: A Comparison with 18F-FDG PET/CT and Histology. Journal of Nuclear Medicine. 2009; 50:959–965. [PubMed: 19443582]
18. Alberts D, Muggia F, Carmichael J, Winer E, Jahanzeb M, Venook A, Skubitz K, Rivera E, Sparano J, DiBella N, Stewart S, Kavanagh J, Gabizon A. Efficacy and safety of liposomal anthracyclines in phase I/II clinical trials. Seminars in Oncology. 2004; 31:53–90. [PubMed: 15717738]
19. Mukundan M, Ghaghada K, Badea C, Kao C, Hedlund L, Provenzale J, Johnson G, Chen E, Bellamkonda R, Annapragada A. A Liposomal Nanoscale Contrast Agent for Preclinical CT in Mice. American Journal of Roentgenology. 2006; 186:300–307. [PubMed: 16423931]
20. Samei E, Saunders R, Badea C, Ghaghada K, Hedlund L, Qi Y, Yuan H, Bentley R, Mukundan S. Micro-CT imaging of breast tumors in rodents using a liposomal, nanoparticle contrast agent. International Journal of Nanomedicine. 2009; 4:277–282. [PubMed: 20011244]
21. Johnston S, Johnson G, Badea C. Geometric calibration for a dual tube/detector micro-CT system. Medical Physics. 2008; 35:1820–1829. [PubMed: 18561657]
22. Badea C, Hedlund L, Johnson G. Micro-CT with respiratory and cardiac gating. Medical Physics. 2004; 31:3324–3329. [PubMed: 15651615]
23. Sun Z, Cao Y. Multislice CT angiography assessment of left coronary artery: correlation between bifurcation angle and dimensions and development of coronary artery disease. Eur J Radiol. 2011; 79:e90–e95. [PubMed: 21543178]
24. Feldkamp L, Davis L, Kress J. Practical cone-beam algorithm. Journal Optical Society America A. 1984; 1:612–619.
25. Badea, C.; Johnston, S.; Qi, Y.; Ghaghada, K.; Johnson, G. Dual-energy micro-CT imaging for differentiation of iodine- and gold-based nanoparticles; Paper presented at: Progress in Biomedical Optics and Imaging - Proceedings of SPIE 7961, art. no. 79611X; Lake Buena Vista, Florida, USA. 2011.
26. Clark D, Johnson GA, Badea CT. Denoising of 4D cardiac micro-CT data using median-centric bilateral filtration. Proceeding of SPIE. 2012; 8314:83143Z.
27. Ghaghada K, Hawley C, Kawaji K, Annapragada A, Mukundan S Jr. T1 Relaxivity of Core-encapsulated Gadolinium Liposomal Contrast Agents—Effect of Liposome Size and Internal Gadolinium Concentration. Academic Radiology. 2008; 15:1259–1263. [PubMed: 18790397]
28. Narula J, Garg P, Achenbach S, Motoyama S, Virmani R, Strauss H. Arithmetic of vulnerable plaques for noninvasive imaging. Nature Clinical Practice Cardiovascular Medicine. 2008; 5(suppl. 2):s2–s10.

29. van Oostrom O, Velema E, Schoneveld A, de Vries J, de Bruin P, Seldenrijk C, de Kleijn D, Busser E, Moll F, Verheijen J, Virmani R, Pasterkamp G. Age-related changes in plaque composition: A study in patients suffering from carotid artery stenosis. Cardiovascular Pathology. 2005; 14:126–134. [PubMed: 15914297]
30. Madjid M, Vela D, Khalili-Tabrizi H, Casscells SW, Litovsky S. Systemic Infections Cause Exaggerated Local Inflammation in Atherosclerotic Coronary Arteries. Texas Heart Institute Journal.: Sepsis and Coronary inflammation. 2007; 34:11–18.
31. Folco E, Sheikine Y, Rocha V, Christen T, Shvartz E, Sukhova G, Di Carli M, Libby P. Hypoxia but not inflammation augments glucose uptake in human macrophages: Implications for imaging atherosclerosis with 18fluorine-labeled 2-deoxy-D-glucose positron emission tomography. Journal of American College of Cardiology. 2011; 58:603–614.
32. Primak AN, Giraldo JCR, Eusemann CD, Schmidt B, Kantor B, Fletcher JG, McCollough C. Dual-Source Dual-Energy CT With Additional Tin Filtration: Dose and Image Quality Evaluation in Phantoms and In Vivo. American Journal of Roentgenology. 2010; 195:1164–1174. [PubMed: 20966323]
33. Ranson M, Carmichael J, O'Byrne K, Stewart S, Smith D, Howell A. Treatment of Advanced Breast Cancer With Sterically Stabilized Liposomal Doxorubicin: Results of a Multicenter Phase II Trial. Journal of Clinical Oncology. 1997; 15:3185–3191. [PubMed: 9336354]
34. Burke S, Annapragada A, Hoffman E, Chen E, Ghaghada K, Sieren J, van Beek E. Imaging of pulmonary embolism and t-PA therapy effects using MDCT and liposomal iohexol blood pool agent: preliminary results in a rabbit model. Academic Radiology. 2007; 14:355–362. [PubMed: 17307669]
35. Ghaghada K, Bockhorst K, Mukundan S, Annapragada A, Narayana P. High-resolution vascular imaging of the rat spine using liposomal blood pool MR agent. American Journal of Neuroradiology. 2007; 28:48–53. [PubMed: 17213423]
36. Ghaghada KB, Badea CT, Karumbaiah L, Fettig N, Bellamkonda RV, Johnson GA, Annapragada A. Evaluation of tumor microenvironment in an animal model using a nanoparticle contrast agent in computed tomography imaging. Academic Radiology. 2011; 18:20–30. [PubMed: 21145026]
37. Chono S, Tauchi Y, Morimoto K. Pharmacokinetic analysis of the uptake of liposomes by macrophages and foam cells in vitro and their distribution to atherosclerotic lesions in mice. Drug Metabolism Pharmacokinetics. 2006; 21:37–44. [PubMed: 16547392]
38. Pan D, Williams T, Senpan A, Allen J, Scott M, Gaffney P, Wickline S, Lanza G. Detecting Vascular Biosignatures with a Colloidal, Radio-Opaque Polymeric Nanoparticle. Jour. Amer. Chem. Society. 2009; 131:15522–155527.
39. Rabin O, Manuel P, Grimm J, Wojtkiewicz G, Weissleder R. An X-ray computed tomography imaging agent based on long-circulating bismuth sulphide nanoparticles. Nature Materials. 2006; 5:118–122.
40. Nakashima Y, Plump A, Raines E, Breslow J, Ross R. ApoE-deficient mice develop lesions of all phases of atherosclerosis throughout the arterial tree. Arteriosclerosis and Thrombosis. 1994; 14:133–140. [PubMed: 8274468]
41. Swirski FK, Nahrendorf M, Etzrodt M, Wildgruber M, Cortez-Retamozo V, Panizzi P, Figueiredo J-L, Kohler RH, Chudnovskiy A, Waterman P, Aikawa E, Mempel TR, Libby P, Weissleder R, Pittet M. Identification of Splenic Reservoir Monocytes and Their Deployment to Inflammatory Sites. Science. 2009; 325:612–616. [PubMed: 19644120]
42. Jawień J, Nastałek P, Korbut R. Mouse models of experimental atherosclerosis. Journal of Physiology and Pharmacology. 2004; 55:503–517. [PubMed: 15381823]
43. Badimon L, Vilahur G, Padro T. Atherosclerosis and thrombosis: insights from large animal models. Journal of Biomedicine and Biotechnology. 2011 Article ID 907575.
44. Szebeni J. The interaction of liposomes with the complement system. Critical Reviews in Therapeutic Drug Carrier Systems. 1998; 15:57–88. [PubMed: 9523086]
45. Cassetta L, Cassol E, Poli G. Macrophage polarization in health and disease. Scientific World Journal. 2011; 11:2391–2402. [PubMed: 22194670]
46. Zeyda M, Stulnig T. Adipose tissue macrophages. Immunol. Lett. 2007; 112:61–67. [PubMed: 17719095]

Commentary

This paper describes the results of a study testing the ability of liposomes to localize in atherosclerotic plaque. Circulating liposomes could localize in the plaques by passive extravasation, or they could be carried there by macrophages that are transported to the plaque. An iodine-containing liposome formulation for maximal macrophage uptake was first optimized in vitro by testing uptake in a macrophage cell line (RAW264.7). In ApoE −/− mice with sizeable plaque buildup, these optimal liposomes, when injected intravenously, readily localized to the plaques, and were detectable and differentiable from calcifications by dual energy CT. The locations of the liposomes within the plaque were measured by imaging cytometry and showed that the liposomes were associated with a small fraction of the macrophages present in the plaques. There was no evidence for liposome localization in the absence of a macrophage in the vicinity. While not conclusive, this data is consistent with the theory of macrophage mediated trafficking and uptake of the liposomes in the plaques.

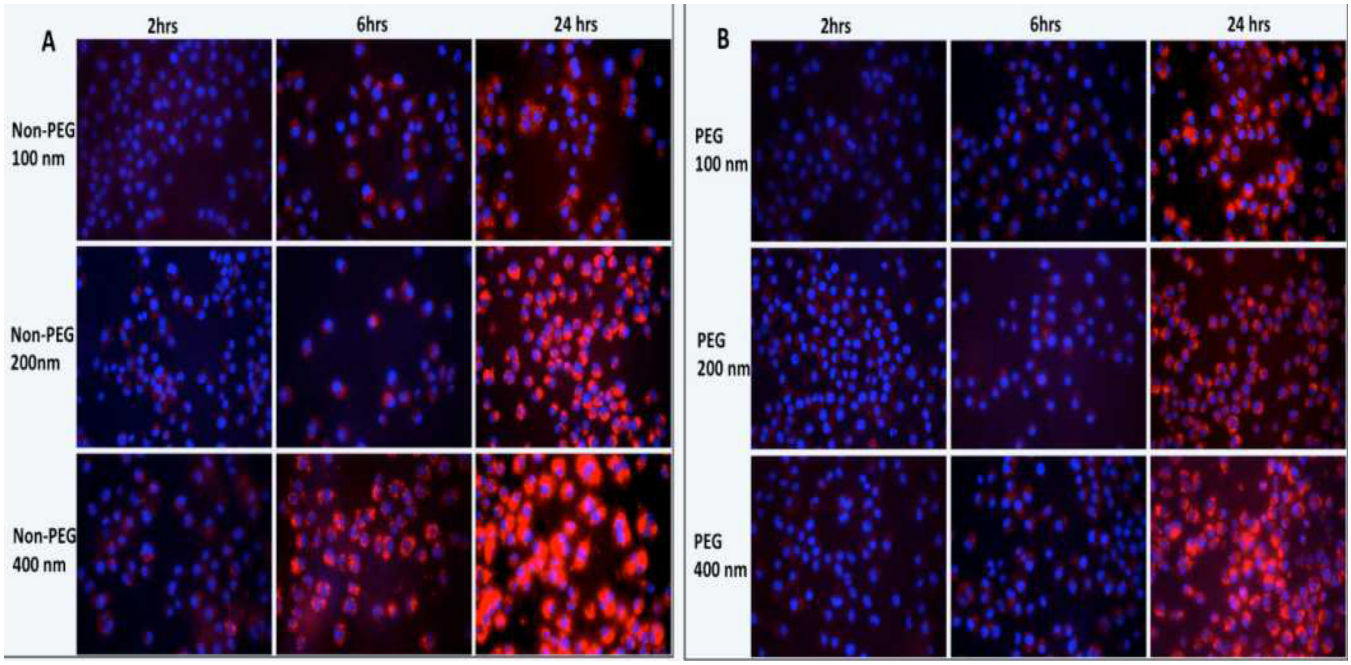

Figure 1.
Effect of liposome size and incubation time on the uptake of rhodamine-labelled non-PEGylated liposomes (A) and PEGylated liposomes (B) by RAW 264.7 macrophages. Cell nucleus was stained with DAPI (blue color). Images were acquired at 40X magnification.

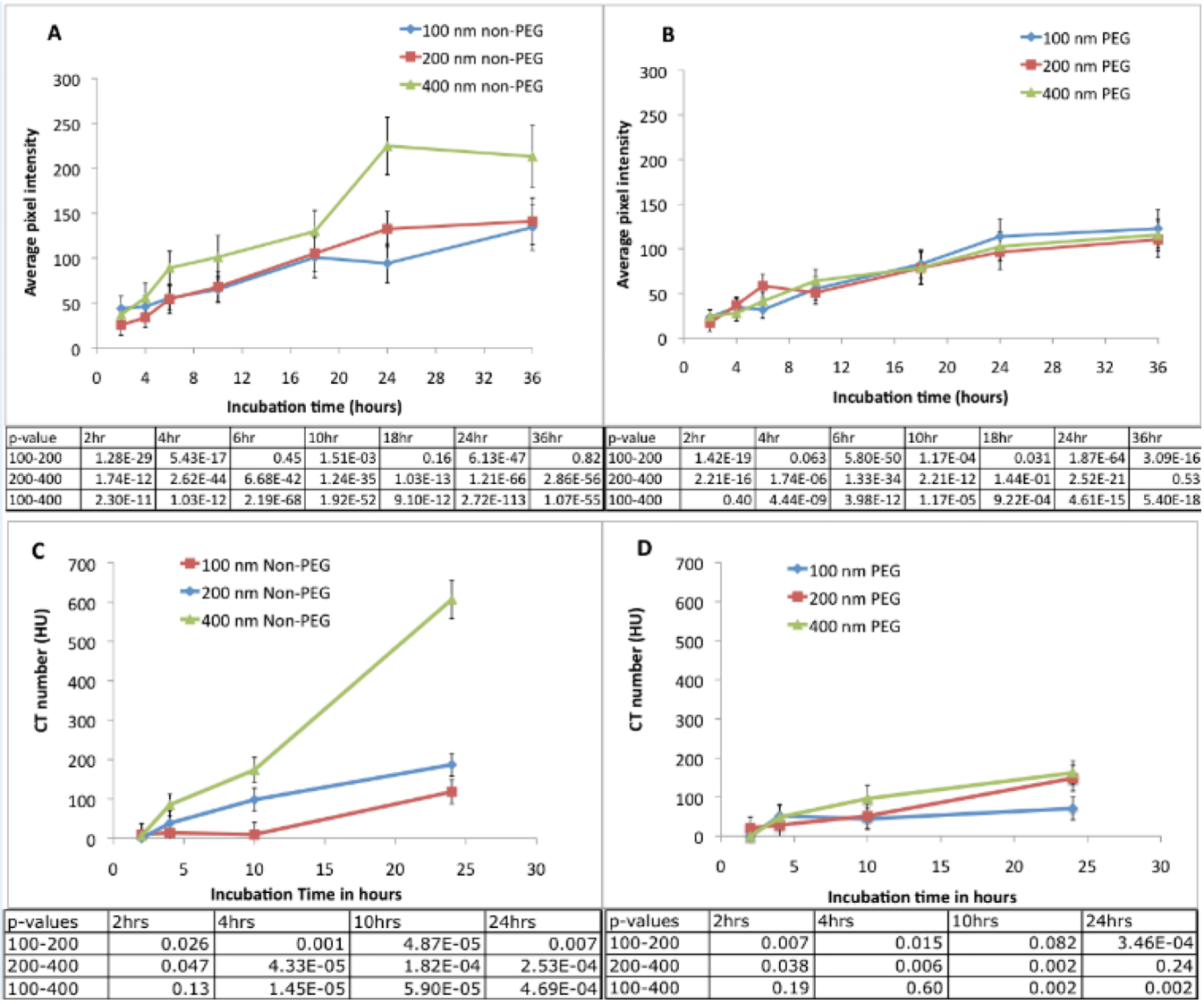

p-value	2hr	4hr	6hr	10hr	18hr	24hr	36hr
100-200	1.28E-29	5.43E-17	0.45	1.51E-03	0.16	6.13E-47	0.82
200-400	1.74E-12	2.62E-44	6.68E-42	1.24E-35	1.03E-13	1.21E-66	2.86E-56
100-400	2.30E-11	1.03E-12	2.19E-68	1.92E-52	9.10E-12	2.72E-113	1.07E-55

p-value	2hr	4hr	6hr	10hr	18hr	24hr	36hr
100-200	1.42E-19	0.063	5.80E-50	1.17E-04	0.031	1.87E-64	3.09E-16
200-400	2.21E-16	1.74E-06	1.33E-34	2.21E-12	1.44E-01	2.52E-21	0.53
100-400	0.40	4.44E-09	3.98E-12	1.17E-05	9.22E-04	4.61E-15	5.40E-18

p-values	2hrs	4hrs	10hrs	24hrs
100-200	0.026	0.001	4.87E-05	0.007
200-400	0.047	4.33E-05	1.82E-04	2.53E-04
100-400	0.13	1.45E-05	5.90E-05	4.69E-04

p-values	2hrs	4hrs	10hrs	24hrs
100-200	0.007	0.015	0.082	3.46E-04
200-400	0.038	0.006	0.002	0.24
100-400	0.19	0.60	0.002	0.002

Figure 2.

Quantitative analysis of uptake of rhodamine-labeled non-PEGylated liposomes (A) and PEGylated liposomes (B) by RAW 264.7 macrophages. A total of 100 cells were used for the analysis. CT number of iodine-containing macrophages (C, D). Macrophages were incubated with non-PEGylated liposomal-iodine (C) and PEGylated liposomal-iodine (D). Error bars represent standard deviations.

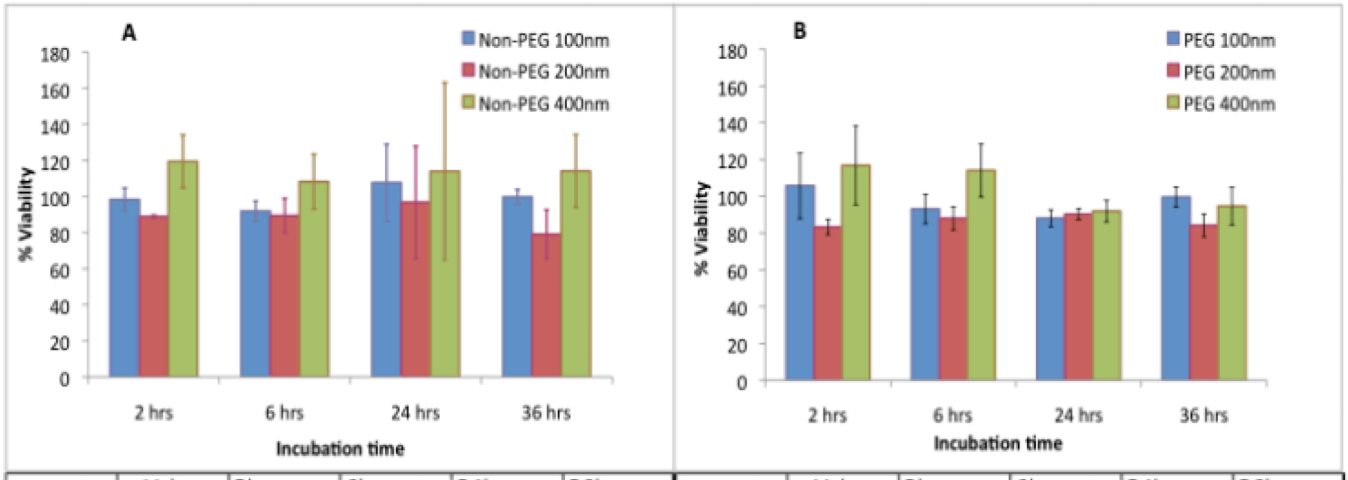

	p-Value	2hrs	6hrs	24hrs	36hrs
NonPEG	100nm	0.75	0.13	0.60	0.97
NonPEG	200nm	0.021	0.18	0.88	0.097
NonPEG	400nm	0.48	0.72	0.95	0.87

	p-Value	2hrs	6hrs	24hrs	36hrs
PEG	100nm	0.64	0.28	0.028	0.92
PEG	200nm	0.005	0.055	0.037	0.020
PEG	400nm	0.74	0.84	0.007	0.071

Figure 3.

Effect of liposomal-iodine uptake on cell viability of RAW 264.7 macrophages. The macrophages were incubated with non-PEG liposomal-iodine (A) and PEGylated liposomal-iodine (B) for different incubation times and the cell viability assessed using the MTS assay. Error bars represent standard deviation. Untreated cells were used as controls and their viability numbers were averaged and normalized to 100%, and all other test cases normalized against this standard.

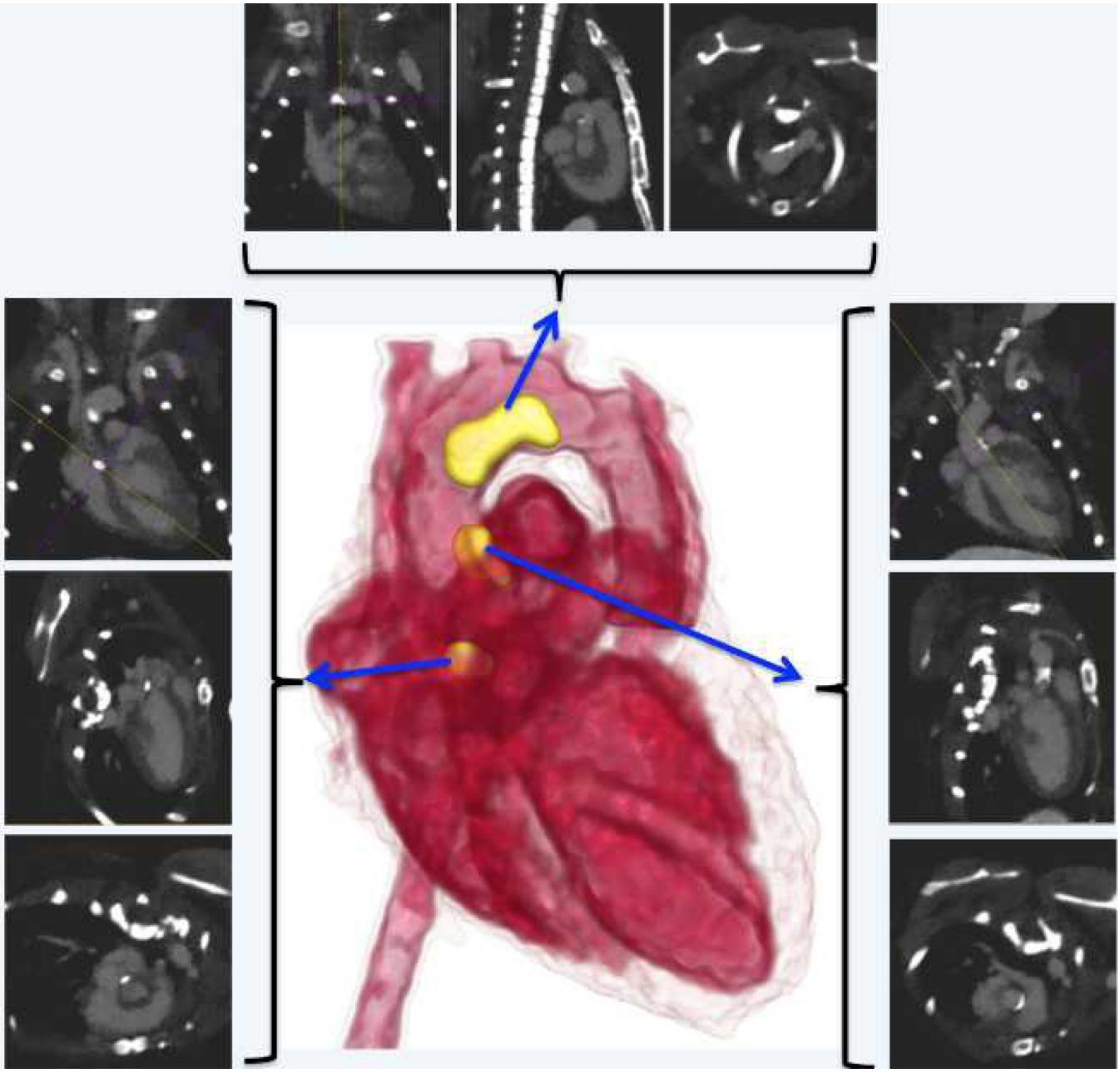

Figure 4.
3D volume-rendered image and orthogonal slices demonstrating co-visualization of blood-pool (red) and calcified plaques (yellow regions) in an ApoE$^{-/-}$ mouse. Images were acquired within 2 hours post-administration of the liposomal contrast agent.

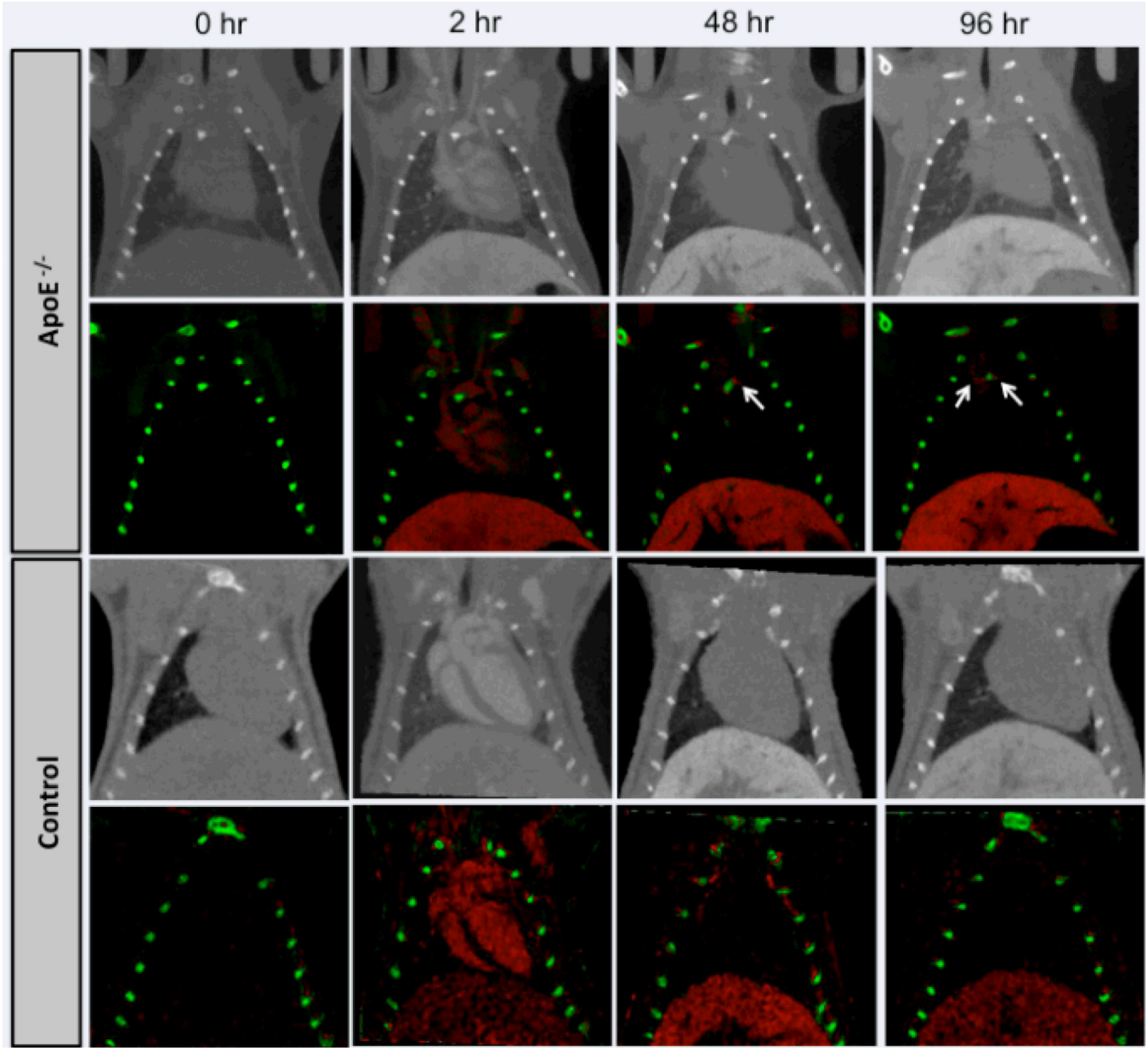

Figure 5.
Representative grayscale (rows 1 and 3) and corresponding decomposed (rows 2 and 4) coronal images of an ApoE$^{-/-}$ and control C57BL/6 mouse before and after administration of liposomal-iodine contrast agent. Red denotes iodine and green denotes calcium. The white arrows indicate region of signal enhancement due to accumulation of liposomal-iodine in plaques.

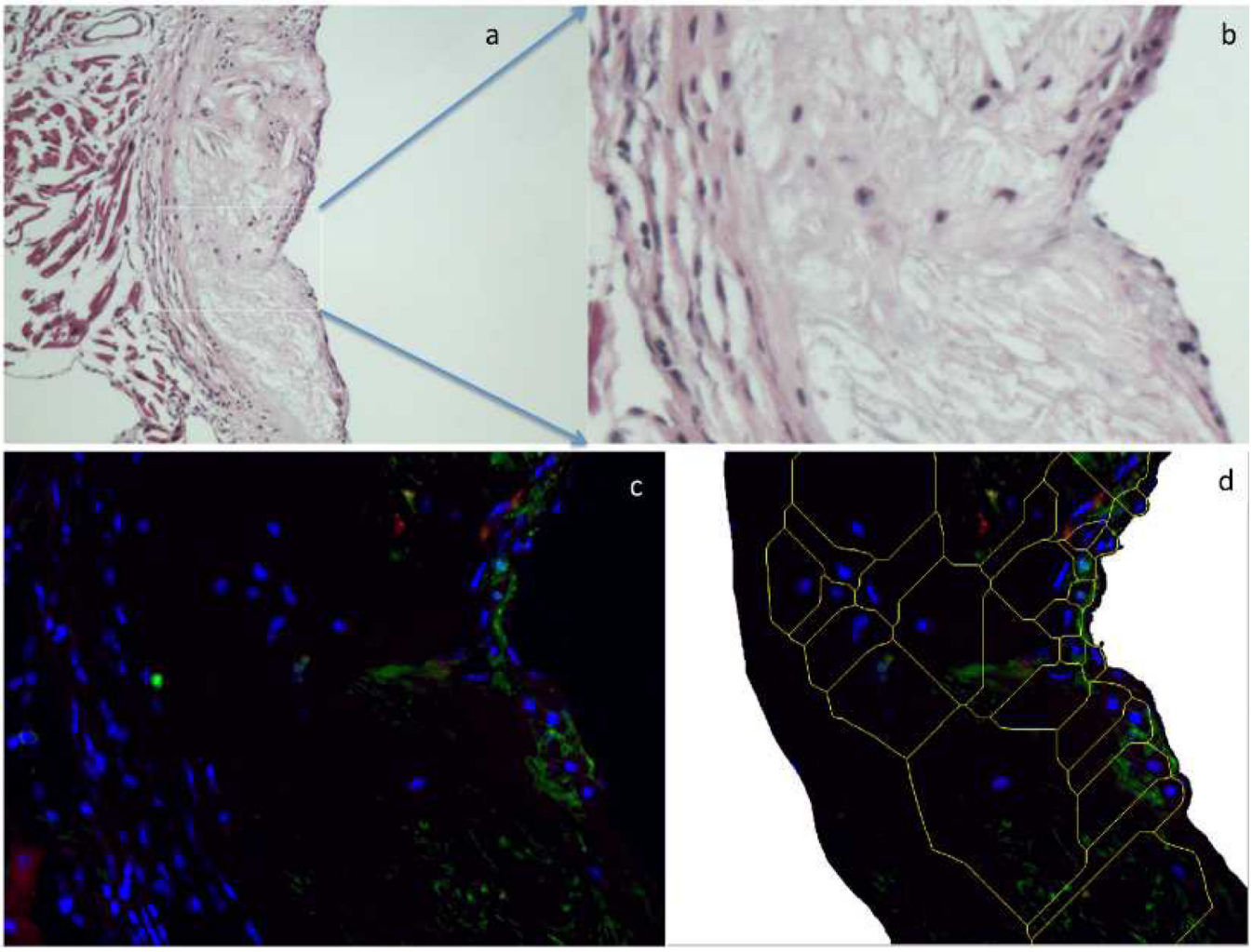

Figure 6.

Histological examination of plaque section showing localization of rhodamine in regions of macrophage infiltration. A: H&E Section showing plaque and vessel wall (tunica media and portions of the adventitia) (10x). B: Inset from A, enlarged. C: DAPI –FITC-rhodamine merged image showing blue: cell nuclei, red: rhodamine in liposomes, green: macrophages labeled by Mac-2 FITC. D: cropped image of *C* used in imaging cytometric analysis, with computer generated tesselation to approximate cell boundaries.

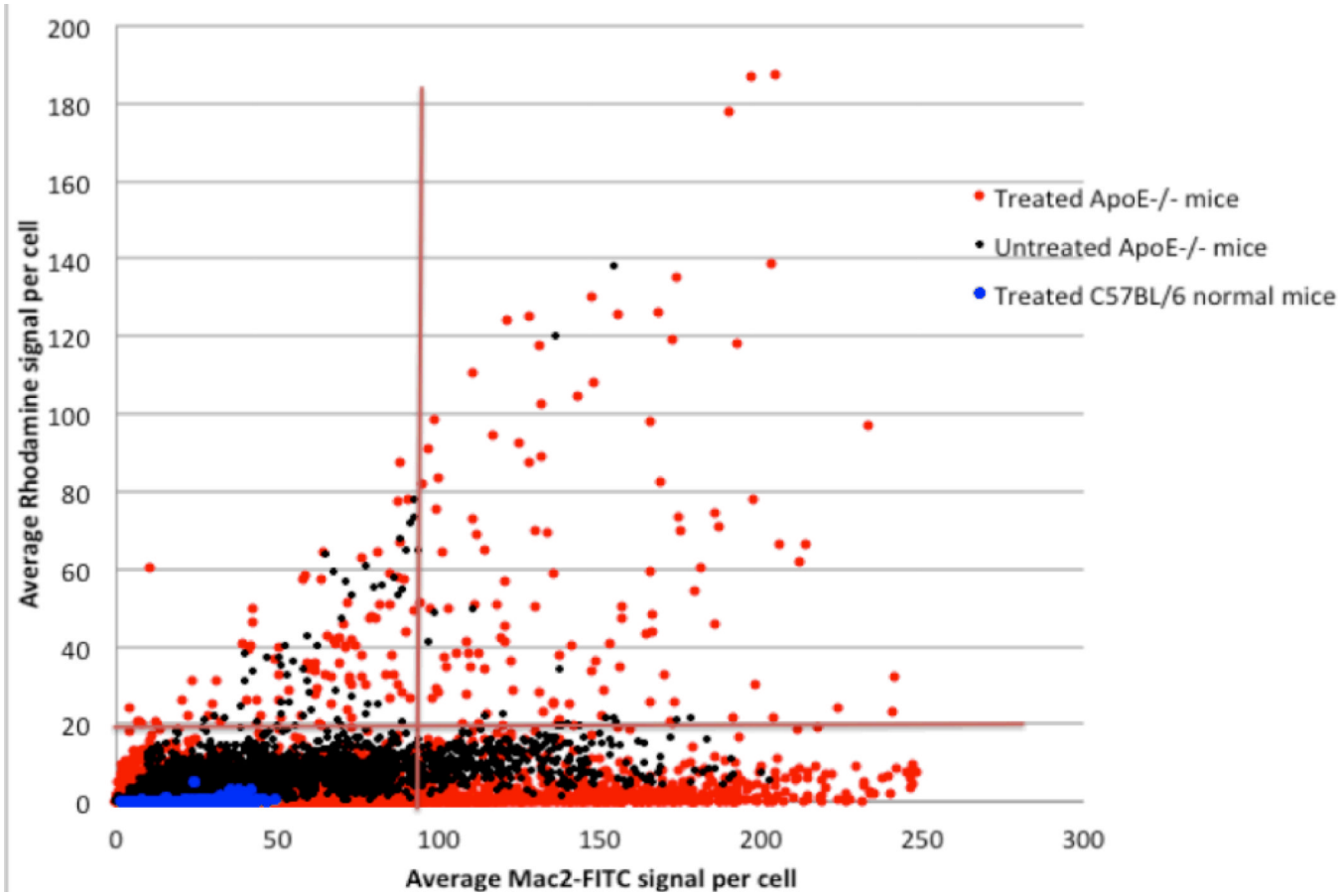

Figure 7.

Imaging cytometric analysis of aorta sections from mice that received rhodamine-labeled liposomes (red dots). ApoE−/− mice with no liposomes (black dots), and background C57BL/6 animals with liposome treatment (blue dots) were used as controls. Note that the C57BL/6 animals show practically no rhodamine or FITC signal, indicating no macrophages and no liposomes in the aortic wall. Untreated ApoE−/− mice show significant FITC signal indicating a significant macrophage level. The corresponding rhodamine signal is attributed to tissue-background and establishes the baseline criterion. The treated ApoE−/− mice show a significant elevation in rhodamine levels for a fraction of the cells (upper right quadrant, ~2% of cells), suggesting that avid uptake of the rhodamine is limited to about 2% of the macrophages in the plaques that are imaged.

Table 1

Description of liposomal preparations

Study	Formulation type	Lipid Composition	Nanoparticle sizes * (nm)	Imaging moiety
In vitro optical imaging	Non-PEG	DPPC:Chol:DPPG:Rh-DHPE – 44.9:35:20:0.1	100, 200, or 400	Rhodamine
	PEG	DPPC:Chol:mPEG-2000-DSPE:Rh-DHPE – 61.9:35:3:0.1	100, 200, or 400	Rhodamine
In vitro CT imaging	Non-PEG	DPPC:Chol:DPPG 45:35:20	100, 200, or 400	Iodine
	PEG	DPPC:Chol:mPEG-2000-DSPE – 62:35:3	100, 200, or 400	Iodine
In vivo CT imaging	Non-PEG	DPPC:Chol:DPPG 45:35:20	400	Iodine and rhodamine

* the numbers 100, 200 and 400 indicate pore sizes of filter membranes through which the liposomes were extruded

Table 2

Size and Zeta potential analysis of liposomal preparations

	Liposome formulation*	Effective diameter in nm (PDI)†	Zeta Potential (mV)
Rhodamine liposomes for in vitro optical imaging	Non-PEG – 100	108 (0.074)	− 81 ± 7
	Non-PEG – 200	166 (0.059)	− 65 ± 2
	Non-PEG – 400	270 (0.177)	− 70 ± 4
	PEG – 100	103 (0.073)	− 36 ± 2
	PEG – 200	146 (0.111)	− 39 ± 2
	PEG – 400	218 (0.125)	− 39 ± 3
Liposomal-iodixanol for in vitro CT imaging	Non-PEG- 100	93 (0.067)	− 58 ± 3
	Non-PEG – 200	144 (0.115)	− 60 ± 2
	Non-PEG – 400	225 (0.121)	− 69 ± 2
	PEG – 100	98 (0.112)	− 37 ± 2
	PEG – 200	119 (0.108)	− 33 ± 2
	PEG – 400	153 (0.071)	− 33 ± 1
Liposomal-iodixanol for in vivo studies	IV-400	172 (0.1)	− 69 ± 1

*the numbers 100, 200 and 400 indicate pore sizes of filter membranes through which the liposomes were extruded.

†PDI is the poly-dispersity index of the particle sizes, defined as the ratio of the volume mean diameter to the number mean diameter.

Table 3

Final iodine concentration assayed by UV absorbance and final lipid concentration determined by phosphorus assay of the phospholipids by ICP-AES

CT liposome formulation	Final Iodine concentration in (mg/ml)	Final Lipid concentration in mg/ml	Final iodine : lipid ratio (mg/mg)
Non PEG – 100	32	38	0.84
Non PEG – 200	69	43	1.6
Non PEG – 400	82	42	1.96
PEG – 100	23	36	0.64
PEG – 200	45	45	0.99
PEG – 400	56	41	1.35
IV-400	70	47	1.47